

Breakdown of Raman Selection Rules By Fröhlich Interaction in Few-Layer WS₂

Qing-Hai Tan¹, Yu-Jia Sun¹, Xue-Lu Liu¹, Kai-Xuan Xu¹, Yuan-Fei Gao^{1,2}, Shu-Liang Ren¹, Ping-Heng Tan^{1,2}, and Jun Zhang^{1,2*}

¹State Key Laboratory of Superlattices and Microstructures, Institute of Semiconductors, Center of Materials Science and Optoelectronics Engineering, CAS Center of Excellence in Topological Quantum Computation, University of Chinese Academy of Sciences, Beijing 100083, China

²Beijing Academy of Quantum Information Science, Beijing 100193, China

*Correspondence and requests for materials should be addressed to J. Z. (zhangjwill@semi.ac.cn)

The Raman selection rules arise from the crystal symmetry and then determine the Raman activity and polarization of scattered phonon modes. However, these selection rules can be broken in resonant process due to the strong electron-phonon coupling effect. Here we reported the observation of breakdown of Raman selection rules in few-layer WS₂ by using resonant Raman scattering with dark A exciton. In this case, not only the infrared active modes and backscattering forbidden modes are observed, but the intensities of all observed phonon modes become strongest under paralleled-polarization and independent on the Raman tensors of phonons. We attributed this phenomenon to the interaction between dark A exciton and the scatted phonon, the so-called intraband Fröhlich interaction, where the Raman scattering possibility is totally determined by the symmetry of exciton rather than the phonons due to strong electron-phonon coupling. Our results not only can be used to easily detect the optical forbidden excitonic and phononic states but also provide a possible way to manipulate optical transitions between electronic levels.

I. INTRODUCTION

Besides the energy and momentum conservation, the Raman scattering processes must follow the so-called Raman selection rules that governed by parities of phonon wavefunctions and hence the symmetry of materials¹. These selection rules are very useful for investigating the Raman activity and polarization property of scattered phonons. Based on Raman selection rules, the infrared (IR) active and Raman active phonons are complementary in centrosymmetric crystals; in some crystals, there are some silent phonon modes which are neither IR nor Raman active, or forbidden in certain scattering geometry. However, these selection rules will be broken under special conditions, such as the electronic field gradient effects of metal plasmonic structure^{2,3} and resonant Raman scattering (RRS) due to strong electron-phonon coupling (EPC)⁴⁻⁶. The EPC plays an important role in thermodynamics, electronic transport and optical properties of solids. Manipulation of EPC will give rise big opportunity to discover new physics phenomena and design novel electronic and optoelectronic devices. Two-dimensional materials (2DMs) and related 2D van der Waals heterostructures (vdWHs) assembled by different 2DMs provide a perfect platform to engineer the EPC, thus to design novel optoelectronic devices⁷⁻⁹. In such 2D system, the EPCs can be dramatically modified and generate many novel physical effects, such as unconventional superconductivity in twisted bilayer graphene¹⁰⁻¹², quantum entanglement between chiral phonon and single photon in WSe₂¹³, cross-dimensional EPC in vdWHs¹⁴, dark-exciton resonance in WS₂⁶, and improving degree of valley polarization by suppress the electron-phonon coupling¹⁵. It is particularly significant to explore Raman selection rules of 2DMs in strong electron-phonon coupling regime, but still elusive so far.

Here we investigated the breakdown of Raman selection rules in few-layer WS₂ by polarization dependent resonant Raman spectroscopy. Multiple laser lines closed to the energies of A, B, and C excitons (electron-hole pairs) of few-layer WS₂ were used to evaluate the resonant behavior of phonons. When the excitation energy is slightly below

bright A exciton state and close to dark A exciton state, a series of IR-active modes and normally forbidden modes in backscattering configuration were clearly observed. In particular, the polarization behaviors of all modes become parallel polarization and independent on the Raman tensor of modes. Experimental and theoretical analysis show that such a breakdown of Raman selection rules originates from intraband Fröhlich interaction between the dark A excitons and scattered phonons.

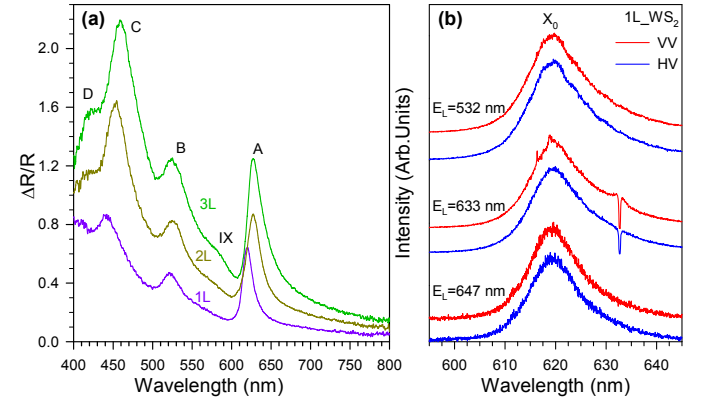


Figure 1 | (a) Reflectance contrast spectra $\Delta R/R$ of 1L, 2L, and 3L WS₂ crystals on SiO₂/Si substrate. (b) The polarized PL spectra of 1L WS₂ with excitation energies close to B, A exciton and slightly below bright A exciton, respectively.

II. EXPERIMENTAL SECTION

The samples were prepared from bulk WS₂ crystals onto a 90 nm SiO₂/Si substrate by using the micromechanical exfoliation technique. Raman measurements were undertaken in backscattering geometry with a Jobin-Yvon HR800 system equipped with a liquid-nitrogen-cooled charge-coupled detector. The spectra were collected with a $\times 100$ objective lens (NA=0.9) and an 1800 lines mm⁻¹

grating at room temperature. The excitation laser (E_L) lines of 457 nm and 488 nm are from an Ar^+ laser; the laser lines of 612 nm and 633 nm are from a He-Ne laser; the laser lines of 532 nm, 647 nm and 676 nm are from a Kr^+ laser. The ultralow-frequency Raman spectra were obtained down to $\pm 5 \text{ cm}^{-1}$ by combining three volume Bragg grating filters into the Raman system to efficiently suppress the Rayleigh signal. In order to avoid the laser heating effect to the samples, the laser power was kept below a maximum of 0.2 mW. The reflectance contrast $\Delta R/R$ were undertaken with a $\times 100$ objective lens ($\text{NA}=0.9$) and an 100 lines mm^{-1} grating with white light at room temperature.

III. RESULTS

Figure 1(a) shows the reflectance contrast spectra $\Delta R/R$ of 1-3L WS_2 at room temperature⁶. Two features at around 627 nm (1.98 eV) and 528 nm (2.35 eV) are denoted by A and B exciton, which originates from direct transitions between the spin-orbit split valence band and the conduction at K (or K') point of the Brillouin zone¹⁶, respectively, the C peak at around 460 nm (2.7 eV) is from transition between the highest valence band and the lowest conduction bands around the Γ point of the Brillouin zone¹⁷. The peak at around 576 nm (2.15 eV) is denoted by IX exciton may correspond to the interlayer exciton of WS_2 or the excitonic Rydberg state of A exciton¹⁸. The origin of D peak at around 413 nm (3.0 eV) is not clear so far. Owing to the direct band gap of monolayer (1L) WS_2 , the energies of A, B and C excitons in 1L are slightly larger than those in bilayer (2L) and trilayer (3L) WS_2 , as shown in Fig. 1(a). Moreover, in contrast to the A and B excitons, C exciton is much less confined to a single layer WS_2 ^{19,20}. Figure 1(b) shows the polarized photoluminescence (PL) spectra of bright A exciton (X_0) in 1L WS_2 with three different laser lines, where one is downconversion PL excited by 532 nm (2.34 eV), another two are upconversion PL excited by 633 nm (1.96 eV) and 647 nm (1.92 eV), respectively. Obviously, the intensities of X_0 peaks are almost the same under parallel (VV) and cross (HV) polarization configurations, implying the bright A exciton is isotropic. It also indicates that its emission and absorption are depolarized for linearly polarized laser. Beside the bright excitons, the conduction band also has a small splitting by tens of meV, which causes the dark A and B exciton transitions^{21,22}. Generally, these dark states lying below the bright states for WS_2 ($X=\text{S}, \text{Se}$), while they are reversed for MoX_2 ^{21,22}. Actually, the dark A exciton of WX_2 has been directly observed by different experiments methods^{23–26}.

To study the polarization behaviors of resonant Raman spectra, we performed the polarized Raman measurements at room temperature with different excitation wavelengths. The intensity of Raman mode can be described as: $I \propto |\mathbf{e}_s \cdot \mathcal{R} \cdot \mathbf{e}_i|$, where \mathcal{R} is the Raman tensor of the vibration mode, \mathbf{e}_i and \mathbf{e}_s are the polarization vectors of the incident and scattered photons, respectively. Considering the backscattering configurations, $\mathbf{e}_i(\mathbf{e}_s)$ can only be along x or y direction, and the corresponding matrix representations are (1, 0, 0) and (0, 1, 0), respectively. The polarization of WS_2 Raman modes is determined by their Raman tensors. The detailed descriptions of Raman ten-

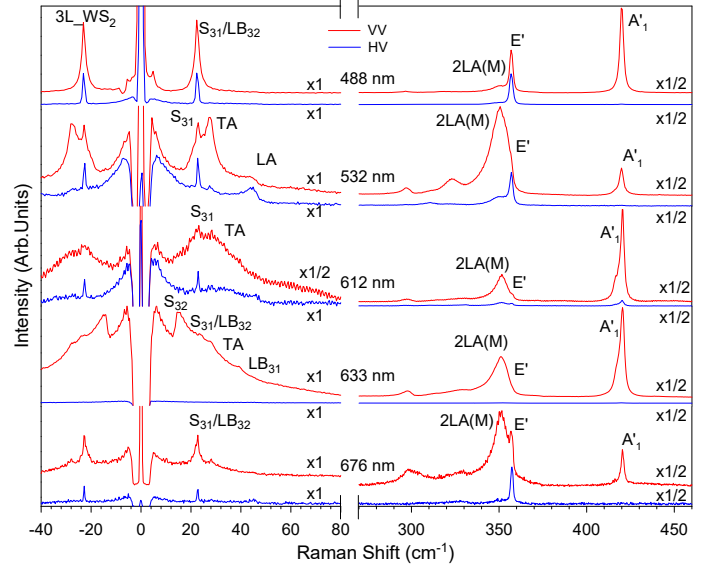


Figure 2 | The polarized Raman spectra of 3L WS_2 with two excitation wavelengths close to C, B exciton and other three excitation wavelengths slighly above, close to and below bright A exciton, respectively.

sors of all modes in WS_2 are presented in Supplementary Information. Figure 2 shows the Raman spectra of 3L WS_2 under parallel (VV) and cross (HV) polarization configurations, where the excitation energies are close to C, B, and A exciton, respectively. Obviously, under resonance with B or C exciton energies, both the in-plane interlayer shear (S) mode and intralayer E' mode survived under VV and HV polarization configurations, whereas out-of-plane interlayer layer breathing (LB) mode and intralayer A'_1 mode only survived under VV configurations, which are consistent with the Raman tensor of these modes. In addition, the LA(M) (177 cm^{-1}) and LA(M)+TA(M) (311 cm^{-1})²⁷ modes are also been observed under both VV and HV polarization configurations, as shown in Figure S1 to Figure S3. It indicates these two modes are not totally polarized under resonance with B or C exciton energies. Remarkably, when the excitation energies are close to bright A exciton energy (around 1.98 eV), some abnormal phenomena were observed. Specifically, when the excitation energy is slightly higher than or far below than bright A exciton energy, for example, 612 nm (2.03 eV) and 676 nm (1.83 eV), these modes still comply with the usual Raman selection rules, similar to the case where the excitation energy is resonant with C and B excitons. However, when the excitation energy is slightly below the bright A exciton energy, such as the excitation using 633 nm (1.96 eV) and 647 nm (1.92 eV) (also see in Figure S4 and S5 of Supplementary Information), besides the Raman active modes, the IR-active (e.g. LB_{31}) and normally backscattering forbidden modes (e.g. both IR and Raman active S_{32}) appear with very strong intensity. The in-plane shear modes (S_{32} and S_{31}) shows Fano line-shape. These phenomena can be well explained based on the parity selection rules due to resonant Raman process involved with dark A exciton⁶. Remarkably, all of the Raman modes show a strong intensity under parallel polarization configurations, but disappear under cross polarization configurations, including LA(M), and in-plane vibration S_{31} and E' modes. For other layers, similar results were also obtained under this resonance con-

dition, as shown in Figure S4 and Figure S5. These abnormal polarization behaviors indicate that Raman selection rules were broken under special resonance conditions.

To further study and confirm this abnormal phonon polarization behavior, we conducted polarization-resolved Raman spectra of 3L WS₂ excited by 488 nm and 633 nm, respectively. We changed the polarization of incident laser by a half-wave plate and fixed the polarizer at the vertical polarization configuration for scattering signals. Figure 3(a-c) show the polarized Raman spectra of 3L WS₂ excited by 488 nm laser. Obviously, the intensities of shear mode and E' mode are independent on the polarization of incident light, while the intensity of A₁' mode is angle-dependent on the polarization of incident light. The evolution of intensities of A₁' modes with polarization angle can be described by $I \propto \cos^2(\beta)$, where β is the polarization angle of excitation laser away from y axis. Figure 3(d-e) show the polarized Raman spectra of 3L WS₂ excited by 633 nm, closing to the energy of dark A exciton. Interestingly, in this case, all modes show the same angle-dependent behavior, including in-plane vibration shear modes, TA and LA(M) modes, and the 2LA(M) and A₁' modes. These results indicate that under 633 nm resonant excitation condition, polarization behaviors of all Raman modes in WS₂ do not follow the symmetry of Raman tensors of vibration modes.

IV. DISCUSSION

As shown above, the forbidden Raman modes and abnormal polarization behavior only were observed under resonance with dark A exciton rather than dark B exciton. This is because that the dark A states are slightly mixed states with bright A exciton. Consequently, the oscillator strength of dark A exciton is quite small but not equal to zero, while the oscillator strength of dark B is strictly equal to zero^{22,28}.

To understand the abnormal polarization behavior of scattered phonons in WS₂ under this resonant condition, we need to analyze it from the first-order Raman scattering cross section^{5,29,30}:

$$\sigma = \sigma_0 \frac{\omega_s}{\omega_i} \left| \sum_{\alpha\beta} \mathbf{e}_s^\alpha \mathcal{R}^{\alpha\beta} \mathbf{e}_i^\beta \right|^2 \quad (1)$$

$$\mathcal{R}^{\alpha\beta} = \sum_{ij} \frac{P_{0j}^\alpha M_{ij} P_{i0}^\beta}{(E_j - \omega_i + \omega_0)(E_i - \omega_s)}$$

where σ_0 is the free-electron Compton cross section $(e^2/mc^2)^2$ and α and β are Cartesian indices, $\omega_{s(i)}$ denotes the frequency of scattered (incident) photons, and E_i and E_j denote the energies of excited electronic states, P_{0i}^α and P_{0j}^β are the momentum matrix element with the ground state 0, M_{ij} is the phonon scattering matrix element, which both the exciton-phonon interaction and exciton-photon interaction are included, ω_0 is the phonon frequency, and \mathbf{e}_i and \mathbf{e}_s are incident and scattered photon polarization. Because the tensorial character of \mathcal{R} determines the polarization selection rules, so we need to consider the expression of \mathcal{R} under resonant condition.

The electron in bright A exciton state will extremely quickly transit to the dark A state by intravalley spin-flip

scattering process with a much faster time scale than radiative recombination, resulting in the low PL quantum yield of monolayer MX₂^{31,32}. In particular, the dark A exciton has a longer radiative lifetime, i.e., two orders of magnitude longer than the radiative lifetime of the bright exciton³³. It will cause the accumulation of electrons in dark A exciton state. Therefore, exciton intraband scattering is dominated by dark state band rather than by bright state band. The dark exciton-phonon interactions here can be described by using intraband Fröhlich interaction^{5,30}. The Hamiltonian $\mathbf{H}_{(F,q)}$ of Fröhlich interaction can be written as³⁴

$$\mathbf{H}_{(F,q)} = iC_F/q [e^{(ip_h \mathbf{q} \cdot \mathbf{r})} - e^{(ip_e \mathbf{q} \cdot \mathbf{r})}] (a_{k+q}^\dagger a_k) (C_{-q}^\dagger + C_q) \quad (2)$$

where $C_F = e[\frac{2\pi\hbar\omega_0}{NV}(\varepsilon_\infty^{-1} - \varepsilon_0^{-1})]^{1/2}(4\pi\varepsilon_0)^{-1/2}$ is a constant coupling coefficient, N and V are the number of unit cells per unit volume of the crystal and the volume of the primitive cell, respectively. $\mathbf{q} = \mathbf{k}_i - \mathbf{k}_s$ is the wave vector of phonon, and ε_0 is the low-frequency optical dielectric constant and ε_∞ is the static dielectric constant. C_q^\dagger and $C_q(a_k^\dagger$ and $a_k)$ correspond to the creation and annihilation operators for phonons (excitons), respectively. The \mathbf{r} is a characteristic length of the excited state. Since the intraband Fröhlich interaction here connects the s states of dark A exciton, the magnitude of the phonon scattering can be simply written as²⁹:

$$M_{ij} = |\langle 1s | \mathbf{H}_{(F,q)} | 1s \rangle|$$

$$= \left(\frac{C_F}{q} \right) \left[\left(\frac{1}{1 + (p_h q r / 2)^2} \right)^2 - \left(\frac{1}{1 + (p_e q r / 2)^2} \right)^2 \right] \quad (3)$$

where $p_e = \frac{m_e}{m_e + m_h}$, $p_h = \frac{m_h}{m_e + m_h}$. For the small but non-negligible q , this magnitude expression can be expanded as

$$M_{ij} \simeq C_F q r \frac{m_e - m_h}{m_e + m_h} \quad (4)$$

Since M_{ij} is a constant only for $i = j$ and is zero for $i \neq j$, the original Raman tensor \mathcal{R} in equation (1) degenerates into a scalar quantity: $\mathcal{R} \propto qr$. This result means that the Raman selection rules are no longer restricted according to Raman tensors and become isotropic (more details are present in Supplementary Information). In this case, if we changed the polarization of incident photon and fixed the polarization of collected signals, i.e., \mathbf{e}_i and \mathbf{e}_s are $[\sin \beta, \cos \beta, 0]$ and $[0, 1, 0]$, respectively, then the Raman intensity can be simply written as:

$$I \propto (qr)^2 \cos^2 \beta \quad (5)$$

It means the intensity of Raman modes is contributes only to diagonal scattering and irrespective of the Raman tensor of phonons. When $\mathbf{e}_i \parallel \mathbf{e}_s$, the Raman intensity reaches the strongest. Obviously, these analyses perfectly explain our polarization dependent experimental results.

V. CONCLUSIONS

In summary, we studied the breakdown effect of strong EPC on Raman selection rules in few-layer WS₂. Under dark A exciton resonance, not only a series of IR-active and backscattering forbidden vibration modes are active,

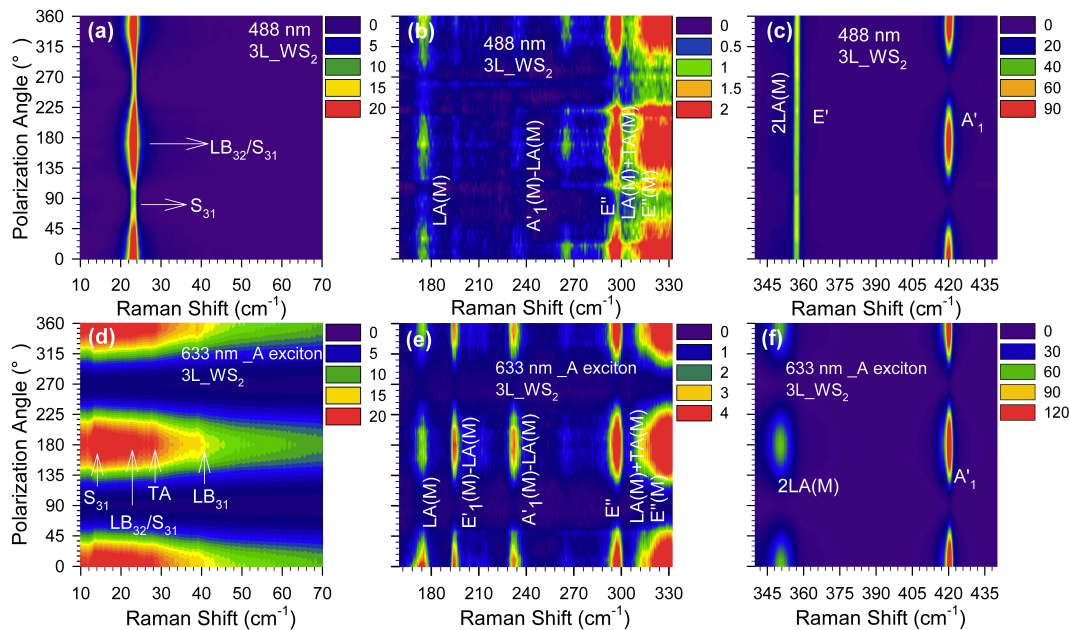


Figure 3 | (a-c) Polarization-resolved Raman intensities of Raman modes in ultralow frequency to high frequency region (including shear mode (S_{31}), layer breathing mode (LB_{31}), and E' and A'_1 modes) in 3L WS_2 under 488 nm, respectively. (d-e) Polarization-resolved Raman intensities of Raman modes in ultralow frequency to high frequency region in 3L WS_2 under 633 nm. To clearly see the evolution of intensities with polarization angle, here we present the data into three separate figures.

but also polarization behaviors of all phonon modes are independent on phonon symmetries. We explained such breakdown of Raman selection rules as intraband Fröhlich interaction of dark A exciton and phonons. In this resonant process, Raman tensor mainly determined by intermediate exciton transition and degenerated into a scalar quantity format, which leads a parallel polarization behavior of all scattered phonon modes. All theoretical results are independent on the crystal symmetry and expected to be observed in other 2DMs and vdWHs. This breakdown the selection rules not only can modulate Raman intensity and polarization, but also increases the optical excitation channels beyond the restriction of selection rules. These characteristic features are expected to provide the significant advantage of controlling the EPC in semiconductors.

Acknowledgements J.Z. and P.T. acknowledge support from National Basic Research Program of China (grant no. 2017YFA0303401, 2016YFA0301200). Beijing Natu-

ral Science Foundation (JQ18014), and Strategic Priority Research Program of Chinese Academy of Sciences (Grant No. XDB28000000).

Author Contribution J.Z. and Q.T. conceived the ideas; Q.T., P.T. and J.Z. designed the experiments. Q.T., X.L., S.R. and Y.S prepared the samples. Q.T. performed experiments. Q.T. and Z.J. analyzed the data and wrote the manuscript with inputs from all authors.

Additional information

Supplementary Information is available in the on-line version of the paper. Correspondence and requests for materials should be addressed to J. Z. (Email: zhangjwill@semi.ac.cn).

Competing interests: The authors declare no competing financial interest.

¹ R. Loudon, Adv. Phys. **13**, 423 (1964)

² E. J. Ayars, H. D. Hallen, and C. L. Jahncke, Phys. Rev. Lett. **85**, 4180 (2000)

³ T. Mai, H. Ajiki, Y. Mizumoto, K. Komeda, M. Nara, H. Nabika, S. Yasuda, H. Ishihara, and K. Murakoshi, Nat. Photonics **7**, 550 (2013)

⁴ P. Y. Yu, Y. R. Shen, Y. Petroff, and L. M. Falicov, Phys. Rev. Lett. **30**, 283 (1973)

⁵ R. M. Martin and L. M. Falicov, "Resonant Raman scattering: Light Scattering in Solids I: Introductory Concepts," (Springer Berlin Heidelberg, Berlin, Heidelberg, 1983) pp. 79–145

⁶ Q. H. Tan, Y. J. Sun, X. L. Liu, Y. Zhao, Q. Xiong, P. H.

Tan, and J. Zhang, 2D Mater. **4**, 031007 (2017)

⁷ H. Zeng and X. Cui, Chem. Soc. Rev. **44**, 2629 (2015)

⁸ C. Jin, E. Y. Ma, O. Karni, E. C. Regan, F. Wang, and T. F. Heinz, Nat. Nanotechnol. **13**, 994 (2018)

⁹ X. Zhang, X. F. Qiao, W. Shi, J. B. Wu, D. S. Jiang, and P. H. Tan, Chem. Soc. Rev. **44**, 2757 (2015)

¹⁰ Y. Cao, V. Fatemi, A. Demir, S. Fang, S. L. Tomarken, J. Y. Luo, J. D. Sanchez-Yamagishi, K. Watanabe, T. Taniguchi, E. Kaxiras, R. C. Ashoori, and P. Jarillo-Herrero, Nature **556**, 80

¹¹ Y. Cao, V. Fatemi, S. Fang, K. Watanabe, T. Taniguchi, E. Kaxiras, and P. Jarillo-Herrero, Nature **556**, 43 (2018)

¹² F. Wu, A. H. MacDonald, and I. Martin, Phys. Rev. Lett.

- 121**, 257001 (2018)
- ¹³ X. Chen, X. Lu, S. Dubey, Q. Yao, S. Liu, X. Wang, Q. Xiong, L. Zhang, and A. Srivastava, *Nat. Phys.* **15**, 221 (2019)
 - ¹⁴ M. L. Lin, Y. Zhou, J. B. Wu, X. Cong, X. L. Liu, J. Zhang, H. Li, W. Yao, and P. H. Tan, *Nature Commun.* **10**, 2419 (2019)
 - ¹⁵ B. Miller, J. Lindlau, M. Bommert, A. Neumann, H. Yamaguchi, A. Holleitner, A. Högele, and U. Wurstbauer, *Nature Commun.* **10**, 807 (2019)
 - ¹⁶ K. F. Mak, C. Lee, J. Hone, J. Shan, and T. F. Heinz, *Phys. Rev. Lett.* **105**, 136805 (2010)
 - ¹⁷ D. Y. Qiu, F. H. da Jornada, and S. G. Louie, *Phys. Rev. Lett.* **111**, 216805 (2013)
 - ¹⁸ J. Horng, T. Stroucken, L. Zhang, E. Y. Paik, H. Deng, and S. W. Koch, *Phys. Rev. B* **97**, 241404 (2018)
 - ¹⁹ B. R. Carvalho, L. M. Malard, J. M. Alves, C. Fantini, and M. A. Pimenta, *Phys. Rev. Lett.* **114**, 136403 (2015)
 - ²⁰ N. Scheuschner, R. Gillen, M. Staiger, and J. Maultzsch, *Phys. Rev. B* **91**, 235409 (2015)
 - ²¹ H. Dery and Y. Song, *Phys. Rev. B* **92**, 125431 (2015)
 - ²² J. P. Echeverry, B. Urbaszek, T. Amand, X. Marie, and I. C. Gerber, *Phys. Rev. B* **93**, 121107 (2016)
 - ²³ M. R. Molas, C. Faugeras, A. O. Slobodeniuk, K. Nogajewski, M. Bartos, D. M. Basko, and M. Potemski, *2D Mater.* **4**, 021003 (2017)
 - ²⁴ Y. Zhou, G. Scuri, D. S. Wild, A. A. High, A. Dibos, L. A. Jauregui, C. Shu, K. De Greve, K. Pistunova, A. Y. Joe, T. Taniguchi, K. Watanabe, P. Kim, M. D. Lukin, and H. Park, *Nature Nanotechnol.* **12**, 856 (2017)
 - ²⁵ G. Wang, C. Robert, M. M. Glazov, F. Cadiz, E. Courtade, T. Amand, D. Lagarde, T. Taniguchi, K. Watanabe, B. Urbaszek, and X. Marie, *Phys. Rev. Lett.* **119**, 047401 (2017)
 - ²⁶ K.-D. Park, T. Jiang, G. Clark, X. Xu, and M. B. Raschke, *Nature Nanotechnol.* **13**, 59 (2018)
 - ²⁷ W. Shi, L. Miao Ling, T. Qing Hai, X. F. Qiao, J. Zhang, and P. H. Tan, *2D Mater.* **3**, 025016 (2016)
 - ²⁸ X.-X. Zhang, T. Cao, Z. Lu, Y.-C. Lin, F. Zhang, Y. Wang, Z. Li, J. C. Hone, J. A. Robinson, D. Smirnov, S. G. Louie, and T. F. Heinz, *Nature Nanotechnol.* **12**, 883 (2017)
 - ²⁹ R. M. Martin and T. C. Damen, *Phys. Rev. Lett.* **26**, 86 (1971)
 - ³⁰ R. M. Martin, *Phys. Rev. B* **4**, 3676 (1971)
 - ³¹ C. Jin, J. Kim, K. Wu, B. Chen, E. S. Barnard, J. Suh, Z. Shi, S. G. Drapcho, J. Wu, P. J. Schuck, S. Tongay, and F. Wang, *Adv. Funct. Mater.* **27**, 1601741 (2017)
 - ³² Z. Wang, A. Molina-Sánchez, P. Altmann, D. Sangalli, D. De Fazio, G. Soavi, U. Sassi, F. Bottegioni, F. Ciccacci, M. Finazzi, L. Wirtz, A. C. Ferrari, A. Marini, G. Cerullo, and S. Dal Conte, *Nano Lett.* **18**, 6882 (2018)
 - ³³ C. Robert, T. Amand, F. Cadiz, D. Lagarde, E. Courtade, M. Manca, T. Taniguchi, K. Watanabe, B. Urbaszek, and X. Marie, *Phys. Rev. B* **96**, 155423 (2017)
 - ³⁴ P. Y. Yu and M. Cardona, "Optical Properties II: Fundamentals of Semiconductors: Physics and Materials Properties," (Springer Berlin Heidelberg, Berlin, Heidelberg, 2010) pp. 345–426